



Contents lists available at ScienceDirect

Arabian Journal of Chemistry

journal homepage: www.ksu.edu.sa

Ultra-light weight proppant of diatomite-reinforced poly(methyl methacrylate-co-styrene) enabling high compressive strength, heat and acid resistance toward hydraulic fracturing

Yuan Zhao ^a, Tao Chen ^a, Li Chen ^b, Guowen Hu ^a, Xiaobing Han ^a, Tian Liang ^{a,*}, Jie Gao ^{a,*}

^a Hubei Key Laboratory of Radiation Chemistry and Functional Materials, School of Nuclear Technology and Chemistry & Biology, Hubei University of Science and Technology, Xianning 437100, China

^b Fourth Geological Team of Hubei Geological Bureau, Xianning 437100, China

ARTICLE INFO

Keywords:

Poly(MMA-co-St)

Diatomite

Reinforcement effect

Thermal barrier effect

ULW proppants

Hydraulic fracturing

ABSTRACT

The growing emphasis on environmental protection in petroleum exploitation results in a high demand for ultra-lightweight (ULW) proppants. This work involves fabricating ULW proppant utilizing suspension polymerization, in which alkyl chain decorated natural clay diatomite (Dia) is incorporated into poly(methyl methacrylate-co-styrene) (poly(MMA-co-St)). The obtained poly(MMA-co-St)/Dia composite beads exhibit a low apparent density ranging from 1.025 to 1.213 g cm⁻³, and show an impressively low crushing rate of 0.99 % under 52 MPa. The rigid and thermally stable Dia crosslinks with poly(MMA-co-St) matrix, which increases the network density and restricts the movement of the molecular chain, thereby enhancing both the mechanical and thermal stability of poly(MMA-co-St)/Dia. Additionally, these composite beads display minimal acid solubility and low turbidity. The exceptional mechanical and thermal stability (attributed to the reinforcement effect and thermal barrier effect of inorganic Dia, as well as the synergistic effect of the copolymerization of MMA and styrene), along with the low acid solubility and turbidity, enabling the poly(MMA-co-St)/Dia composite to replace traditional proppants and be applied in hydraulic fracturing for oil and gas exploitation.

1. Introduction

Taking environmental protection into consideration, hydraulic fracturing is a highly efficient and extensively utilized technique for enhancing the efficiency of extracting petroleum and gas from reservoirs (Yao et al., 2022). The proppant plays a crucial role in hydraulic fracturing, maintaining conductive fractures and significantly enhance the efficiency of oil and gas extraction, especially for old wells and low permeability reservoirs (Liang et al., 2016). The proppants are usually required to function effectively over several kilometers underground, enduring harsh conditions such as high pressure, high temperature, and corrosive chemicals (Zhang et al., 2016). The ideal proppants should possess a density comparable to water, strength equivalent to diamond, and be cost-effective like soil. The acquisition of a proppant possessing all these ideal properties, however, presents a significant challenge (Pangilinan et al., 2016).

Proppants that are used in conventional extraction of petroleum and gas include natural sand (Fjaestad and Tomac, 2019), resin-coated sand

(Fu et al., 2016, Ramlan et al., 2022), synthetic ceramics (Ma et al., 2019a), and coated ceramics (Zhang et al., 2016). All of them can withstand the closure stress of petroleum and gas reservoir. The high density of these proppants, however, impedes fracture propagation, thereby diminishing crack filling efficiency and fracture conductivity, ultimately compromising the effectiveness of oil and gas extraction (Gaurav et al., 2012, Mao et al., 2020). The ultra-lightweight (ULW) proppants provide a solution to these challenges by enhancing fracture conductivity while not hindering fracture propagation, thereby enabling efficient petroleum extraction from reservoirs. This is particularly beneficial in old wells and low permeability reservoirs where conventional proppants may be less effective (Posey and Strickland, 2005, Gaurav et al., 2010, Spurr et al., 2017). Consequently, the development and utilization of ULW proppants have become imperative in the petroleum industry for improving extraction efficiency and optimizing production processes.

The suspension polymerization process can realize the production of ULW proppants. The crosslinked polystyrene beads based proppants was

* Corresponding authors.

E-mail addresses: liangtian@hbust.edu.cn (T. Liang), gaojie2019@hbust.edu.cn (J. Gao).

<https://doi.org/10.1016/j.arabjc.2024.105768>

Received 24 January 2024; Accepted 29 March 2024

Available online 30 March 2024

1878-5352/© 2024 Published by Elsevier B.V. on behalf of King Saud University. This is an open access article under the CC BY-NC-ND license (<http://creativecommons.org/licenses/by-nc-nd/4.0/>).

reported for the first time by our group, wherein graphite was incorporated into polystyrene matrix to enhance the strength and heat resistance (Han et al., 2014). Currently, ULW proppants produced through suspension polymerization have been extensively investigated and implemented.

Due to the high modulus and excellent chemical resistance, various poly(methyl methacrylate) (PMMA) beads based proppants have been developed, such as graphite/PMMA (Chen et al., 2015), carbon black/PMMA (Liang et al., 2017b), silica fume/PMMA (Wang et al., 2015), fly ash/PMMA (Zhang et al., 2015), etc. Meanwhile, polystyrene (PS) demonstrates exceptional compressive strength and wear resistance, and numerous researches have been conducted on incorporating different fillers into PS to synthesize beads based proppants, including graphite (Han et al., 2014), carbon black (Ma et al., 2019b), carbon nanotube (Tasqué et al., 2021), silica fume (Liang et al., 2017), etc. However, PMMA exhibits a relatively low abrasion resistance and PS possesses a low modulus, limiting their potential applications (Huang et al., 2010, Wang et al., 2015, Liang et al., 2017a). Fortunately, the PS displays excellent abrasion resistance while PMMA demonstrates a high modulus, which can compensate for the aforementioned drawbacks of PMMA/PS. The copolymerization of MMA and St (poly(MMA-co-St)) may overcome the limitations of the monomers through their synergistic effect, thereby achieving not only enhanced modulus but also enlarged compressive strength and wear resistance. Meanwhile, there are few reports on poly(MMA-co-St) composite-based proppants.

Herein, we report the development of ULW proppant by leveraging the reinforcement effect and thermal barrier effect of Dia, along with robust bonding between modified Dia and poly(MMA-co-St). Specifically, Dia is firstly modified with alkyl chain. The modified Dia is then well dispersed in a solution containing MMA and St, and further copolymerized to form a poly(MMA-co-St)/Dia composite. The strong crosslinking between the poly(MMA-co-St) and modified Dia results in a high interfacial shear strength, which leads to a low crushing rate of poly(MMA-co-St)/Dia. The modified Dia serves as the thermal barrier and forms crosslink with the polymer chain, increasing the network density and impeding the molecular motion of poly(MMA-co-St)/Dia, resulting in enhanced thermal stability. Overall, the obtained poly(MMA-co-St)/Dia composite beads demonstrate significant potential for utilization as ULW proppants in hydraulic fracturing.

2. Materials and methods

2.1. Materials

Diatomite (Dia) was provided by Aladdin Reagent (Shanghai) Co., Ltd. Stearic acid (SA) was purchased from Shanghai Macklin Biochemical Technology Co., Ltd (Shanghai, China). Methyl methacrylate (MMA), styrene (St), divinyl benzene (DVB), benzoyl peroxide (BPO), (3-aminopropyl)triethoxysilane (APTES), and methanol were purchased from Sinopharm Chemical Reagent Co., Ltd.(China). $\text{MgCl}_2 \cdot 6\text{H}_2\text{O}$, NaOH, and polyvinyl alcohol (PVA) were purchased from Tianjin Fuchen Chemical Regents Factory (China). Deionized water was used throughout the experiments.

2.2. Modification of diatomite

120 mL of toluene was added to a 250 mL flask, followed by adding APTES and Dia at a weight ratio of 4:100. The mixture was then mechanically stirred for 2 h at 90 °C. After that, the SA was added and dissolved, refluxed at 90 °C and stirred for 2 h. The weight ratio of SA to Dia was 4:100. The product was filtered, washed with deionized water and absolute ethanol, and then dried at 60 °C.

2.3. Synthesis of poly(MMA-co-St)/Dia composite proppant

The preparation procedure is as follows:(Chen et al., 2021) 0.4 g PVA

was added to deionized water (80 mL) and stirred at 60 °C for 0.5 h. Subsequently, 4.0 g $\text{MgCl}_2 \cdot 6\text{H}_2\text{O}$ and 1.6 g NaOH were introduced and stirred for 10 min, which was referred to as solution A. The following components were sequentially added to a beaker and stirred: 10.0 g MMA, 10.0 g St, 3.0 g DVB, a specific quantity of modified Dia (the mass was calculated by multiplying a certain percentage with the combined masses of MMA and St), and 0.3 g BPO. This mixture was referred to as solution B. Next, solution B was added into solution A, stirred at 290 r min^{-1} and heated at 78 °C for 1 h, then maintained at 85 °C for 2 h, and lastly heated at 90 °C for 2 h. The product was filtrated, washed with deionized water and methanol, and dried at 60 °C. The control samples of pure PMMA, PS, and poly(MMA-co-St) microspheres were also prepared through a similar procedure. The composite beads with the particle size of 20–40 mesh were adopted as the research object.

2.4. Characterization

The polymer beads were initially pulverized into fine powder. The powder was then washed with ethanol to dissolve residual monomers or reaction byproducts. After being washed with ethanol, the sample was filtered to separate polymer solids from ethanol, effectively eliminating soluble impurities. The filtered polymer solids were subsequently subjected to a thorough drying process in order to eliminate any residual solvent and ensure the sample achieved complete dryness prior to infrared analysis. Fourier transform infrared (FTIR) spectra were recorded on an Avatar 360 Nicolet instrument (Thermo Fisher Scientific, Shanghai, China). Powder X-ray diffraction (XRD) patterns were performed using a Rigaku Multiflex powder diffract meter with Cu radiation. The optical microscope (Olympus CX43) was adopted to facilitate the visualization of surface morphology, particle size distribution, and overall physical appearance of the proppants. The morphologies were observed by a scanning electron microscopy (FESEM, Hitachi SU8010, Japan). The energy-dispersive X-ray spectroscopy (EDS) spectra were acquired at 20 kV with a resolution of 127.4 eV. The density was calculated by the ratio of mass to volume with a 50 mL pycnometer based on SY/T5108-2014. The crush resistance was measured using a WAW100D microcomputer-controlled electro-hydraulic servo universal testing machine (Jinan Hengsi Instruments Co. Ltd) under room temperature (~30 °C). The thermogravimetry analysis (TGA) was conducted via a NETZSCH TG 209 F3 instrument (NETZSCH Scientific Instruments Trading, Ltd., Shanghai, China) under air from room temperature to 600 °C at a heating rate of 10 °C min^{-1} . The DSC curves of the polymer composite beads were obtained using a differential scanning calorimeter (DSC 200 F3, NETZSH) with a nitrogen flow rate of 20 mL min^{-1} and a heating rate of 10 °C min^{-1} . The acid solubility and turbidity were determined according to the Chinese Petroleum and Gas Industrial Standard (SY/T 5108-2006).

3. Results and discussion

The synthesis procedure of diatomite-reinforced copolymer (poly(MMA-co-St)/Dia) is depicted in Fig. 1. The inorganic diatomite (Dia) is first functionalized with amino groups using APTES, which has a triethoxysilane group ($-\text{Si}(\text{OC}_2\text{H}_5)_3$) and an amino group ($-\text{NH}_2$). In the presence of water, the triethoxysilane group hydrolyzes to form silanol groups ($-\text{Si}-\text{OH}$), which then undergo condensation reactions with surface silanol groups on the SiO_2 of diatomite. This forms covalent bonds (siloxane bond of $-\text{Si}-\text{O}-\text{Si}-$) between APTES molecules and the diatomite surface, while also providing amino groups on the diatomite surface (Gutiérrez Moreno et al., 2020, Wu et al., 2022).

Secondly, the amino-functionalized diatomite is modified with stearic acid. During this step, carboxyl groups ($-\text{COOH}$) in stearic acid react with amino groups on the APTES-grafted diatomite surface to form amide bonds ($-\text{CO}-\text{NH}-$), covalently attaching stearic acid molecules to the diatomite surface. This process introduces the alkyl chain of stearic acid molecules onto the APTES-modified diatomite surface, resulting in

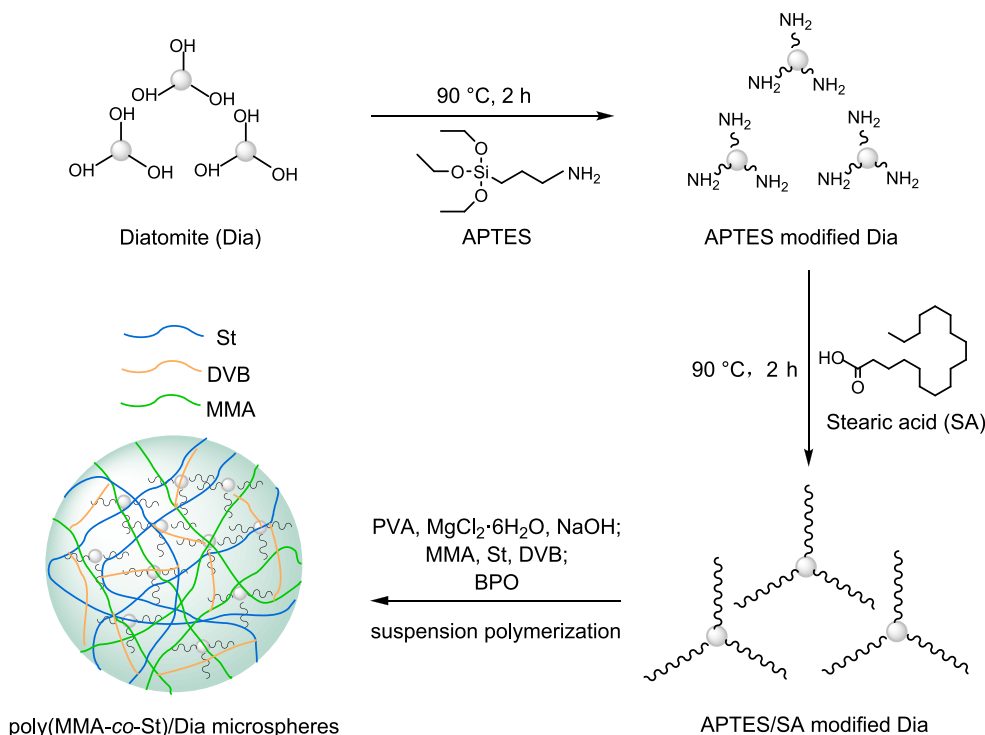


Fig. 1. The synthesis procedure of diatomite-reinforced copolymer composite beads (poly(MMA-co-St)/Dia).

its hydrophobicity (Wang et al., 2015).

Thirdly, the alkyl chain-decorated diatomite particles are dispersed in an aqueous solution containing polyvinyl alcohol (PVA), MgCl₂·6H₂O, NaOH, methyl methacrylate (MMA), styrene (St), divinylbenzene (DVB), and benzoyl peroxide (BPO). The mixture undergoes heating and polymerization to form poly(MMA-co-St)/Dia composite beads. During this process, the hydrophobic alkyl chain-decorated diatomite particles adsorb into the monomer droplets. The PVA, along with MgCl₂·6H₂O and NaOH, functions as a stabilizer in suspension polymerization to maintain reaction mixture stability and promote uniform droplet formation (Chaudhary and Sharma, 2019). Polymerization starts when BPO decomposes upon heating to generate free radicals that initiate the reaction (Salisu et al., 2015). These radicals attack monomer double bonds, initiating polymerization by adding monomer units to growing chains. DVB serves as a cross-linking agent during this process by introducing cross-links between polymer chains (Huang et al., 2010, Sun and Pan, 2010). The reaction terminates when free radicals are consumed or deactivated through various mechanisms such as combination termination or disproportionation termination (Xu et al., 2023). Throughout these steps, alkyl chain-modified diatomite particles are effectively dispersed within a three-dimensional network structured polymer chains, leading to the formation of poly(MMA-co-St)/Dia composite beads.

3.1. Morphological analysis

The suffix of the sample name denotes the weight percentage of the incorporated diatomite, with “weight” referring to the combined mass of MMA and St. The optical microscope images of poly(MMA-co-St), poly(MMA-co-St)/20 wt% Dia, and poly(MMA-co-St)/40 wt% Dia all show a uniform size distribution (Fig. 2). The poly(MMA-co-St) beads demonstrate a smooth surface and pearly luster in their optical images, with an approximate diameter of 0.6 mm. The addition of Dia leads to a rougher surface of the composite beads (Liang et al., 2017). The composites containing 20 wt% Dia exhibit a translucent appearance, whereas those with 40 wt% Dia result in the formation of opaque white beads. It can be ascribed that at higher Dia concentration, the increased density and clustering of Dia particles within the beads can lead to greater light scattering, resulting in reduced transparency and the opaque white appearance. The sphericity of the poly(MMA-co-St)/Dia composite beads is observed to exceed 0.9, which demonstrates a significant improvement compared to that of natural sand (0.65), resin-coated sand (0.8), and ceramic proppants (0.85) (Han et al., 2014, Zhang et al., 2015). The sphericity of the proppants is determined by referring to the Krumbien/Sloss chart (Figure S1, Supporting Information). The high sphericity of the proppant can enhance the porosity of the pack, thereby promoting the conductivity of oil and gas flow (Michael et al., 2020,



Fig. 2. Optical images of (a) poly(MMA-co-St), (b) poly(MMA-co-St)/20 wt% Dia, and (c) poly(MMA-co-St)/40 wt% Dia.

Danso et al., 2021). The PS and PMMA beads are prepared for comparison, all of which demonstrate a transparent appearance (Figure S2, Supporting Information).

Scanning electron microscope (SEM) is employed to characterize the microstructure of the samples. Similar to the optical microscope images, the poly(MMA-co-St), poly(MMA-co-St)/20 wt% Dia (Fig. 3), and poly(MMA-co-St)/40 wt% Dia (Figure S3, Supporting Information) all exhibit a consistent size distribution and excellent sphericity. Additionally, the Dia particles display a random distribution across the surface of poly(MMA-co-St)/20 wt% Dia and poly(MMA-co-St)/40 wt% Dia, proving their effective embedding within the copolymer matrix. The cross-sectional images of the poly(MMA-co-St)/30 wt% Dia further confirm the successful incorporation of diatomite into the polymer matrix of poly(MMA-co-St) (Figure S4, Supporting Information). To investigate the composition of the polymer beads, three distinct regions (Figure S5, Supporting Information) are selected for analysis of the energy-dispersive X-ray spectroscopy (EDS) spectra (Figure S6, Supporting Information), further obtaining the table for “eZAF smart quant results with oxides” (Table S1, Supporting Information). The results indicate that the combined mass of SiO₂ and Al₂O₃ (main components of diatomite) constitutes 28.9 wt% of the polymer beads, exhibiting a close resemblance to the composition of poly(MMA-co-St)/30 wt% Dia.

3.2. Molecular and crystalline structure

The FTIR is adopted to identify the functional groups in the samples. In the spectrum of pure PMMA (Fig. 4a), characteristic peaks corresponding to the C-O stretching vibration (1147 cm⁻¹), ester group of C=O (1729 cm⁻¹), as well as stretching vibrations of -CH- (2951 cm⁻¹), -CH₂- (2843 cm⁻¹), and -CH₃ (2995 cm⁻¹) can be observed (Chen et al., 2015, Liang et al., 2017). The spectrum of pure PS exhibits prominent peaks corresponding to C-H bending vibration (701 and 757 cm⁻¹), stretching of the aromatic skeleton (1452, 1493, and 1601 cm⁻¹), and

stretching of aromatic C-H bonds (3025 cm⁻¹) (Han et al., 2014, Ma et al., 2019). The spectrum of poly(MMA-co-St) display characteristic peaks associated with both PMMA and PS, indicating the successful formation of copolymer beads (Chen et al., 2021). New peaks that correspond to the Si-O-Si bending (479 cm⁻¹) and stretching (1098 cm⁻¹) vibration can be recognized in the spectrum of poly(MMA-co-St)/20 wt% Dia composite, revealing the successful incorporation of modified Dia into the copolymer matrix. The spectra of PS, PS/Dia, PMMA, and PMMA/Dia all exhibit the characteristic peaks of PS, PMMA, Dia or their combination as mentioned above (Figure S7, Supporting Information).

The crystallographic structure of materials can be analyzed using X-ray Diffraction (XRD). The pattern of Dia (Fig. 4b) displays characteristic planes at 101, 110, and 200 corresponding to quartz (JCPDS No.46-1045), as well as characteristic planes at 111, 102, and 301 associated with cristobalite (JCPDS No.39-1425), proving that Dia predominantly consists of quartz and cristobalite (Zheng et al., 2018). The poly(MMA-co-St) exhibits no discernible peaks except for a prominent broad peak within the range of 10 to 25°, suggesting its amorphous nature (Bhanvase et al., 2012, Bernardo et al., 2017). The patterns of poly(MMA-co-St)/20 wt% Dia and poly(MMA-co-St)/40 wt% Dia illustrate a broad peak and multiple sharp peaks, which are attributed to the amorphous copolymer and crystalline Dia, respectively, confirming the well integration of copolymer and modified Dia. Besides, the peak intensity of the corresponding crystal phase in the poly(MMA-co-St)/40 wt% Dia is enhanced with the incremental addition of diatomite. The XRD patterns of PS/Dia and PMMA/Dia also display broad peak and multiple sharp peaks that correspond to amorphous polymer and crystalline Dia (Figure S8, Supporting Information).

3.3. Density and mechanical stability

Fig. 5a presents the apparent density and bulk density of poly(MMA-

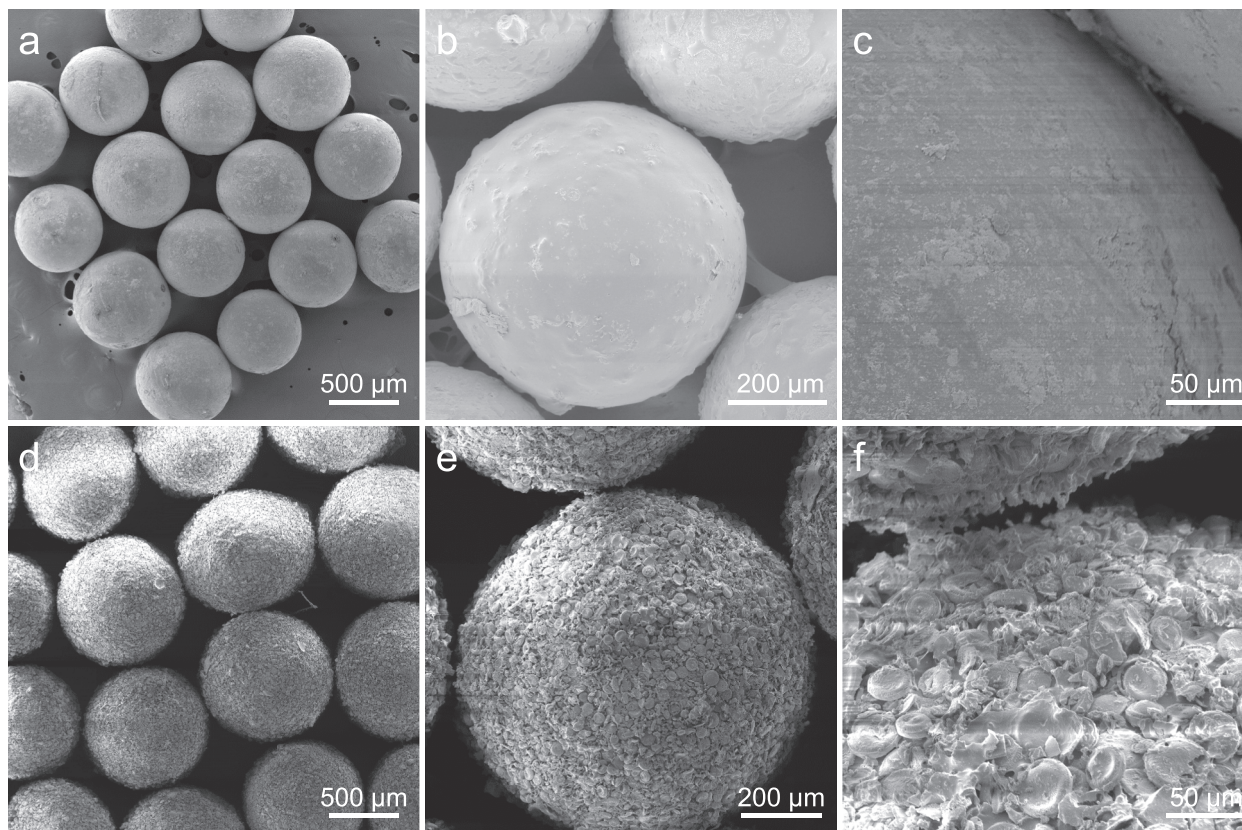


Fig. 3. SEM images of (a-c) poly(MMA-co-St) and (d-f) poly(MMA-co-St)/20 wt% Dia.

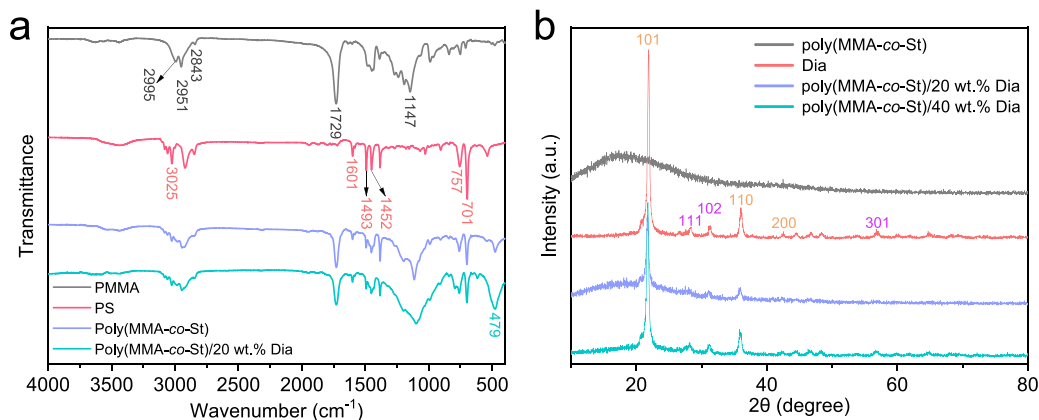


Fig. 4. (a) FTIR spectra and (b) XRD patterns of different samples.

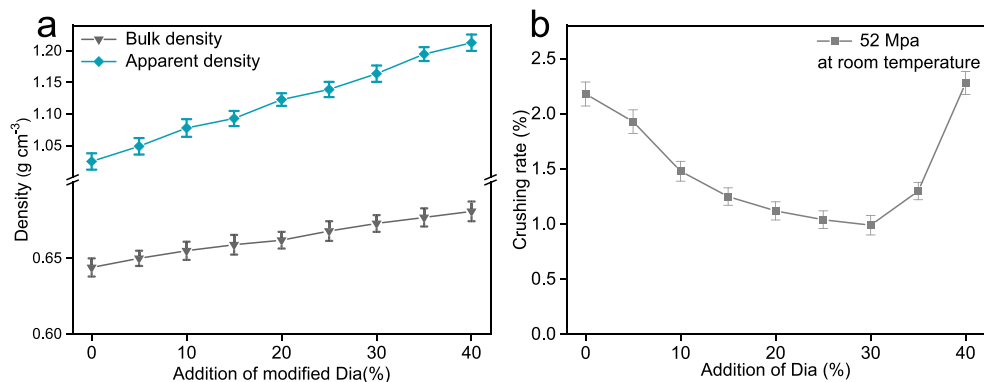


Fig. 5. Properties of poly(MMA-co-St)/Dia composite beads containing different amounts of Dia: (a) apparent density and bulk density, (b) crushing rate under 52 MPa at room temperature (~ 30 °C).

co-St)/Dia composite beads containing varying amounts of Dia. Apparent density represents the density of the material's solid phase without considering any void spaces, while bulk density includes the spaces between particles and voids within the material. Results show that as the content of Dia increases from 0 to 40 wt%, the apparent density of the composite beads also rises from 1.025 to 1.213 g cm^{-3} , all falling within the defined range for ULW proppant. When utilizing high-density proppants in the fracturing process, it becomes imperative to enhance the displacement or viscosity of the fracturing fluid, thereby giving rise to challenges such as intricate management of fluid backflow and substantial reservoir impairment (Ma et al., 2019, Feng et al., 2021). Therefore, the ultra-low density property makes the obtained composite beads ideal for hydraulic fracturing, surpassing both natural sand (2.65 g cm^{-3}) and synthetic ceramic (3.25 g cm^{-3}) proppant (Chen et al., 2015).

To accustom to the high-pressure working environment underground, the ULW proppant should possess a high compressive strength (Michael et al., 2020, Danso et al., 2021, Liao et al., 2022). The compressive strength of the composite beads was assessed by measuring their crushing rate under 52 MPa, as depicted in Fig. 5b. The results indicate that the crushing rate of the beads initially decreases and then increases with the addition amount of Dia escalates, reaching a minimum crushing rate of 0.99 % at an addition amount of 25 wt%.

The initial decrease in the crushing rate of poly(St-co-MMA)/Dia composite beads as the Dia content increases can be attributed to the following reasons. (1) High interfacial shear strength: The bonding of crosslink between the poly(MMA-co-St) matrix and Dia results in a high interfacial shear strength. This bonding prevents the expansion of cracks inside the composite beads, leading to a decrease in the crushing rate. (2) Crack expansion transfer: The good bonding between the poly(MMA-

co-St) matrix and Dia allows the expansion of a crack to be transferred. This transfer mechanism helps to distribute the stress and reduces the likelihood of crack propagation, contributing to a lower crushing rate. (3) Stiffness improvement: The incorporation of hard Dia powders into the poly(MMA-co-St) matrix improves the stiffness of the composites. This improvement restricts the movement of the matrix molecular chain, making the beads more resistant to crushing (Michael et al., 2020, Danso et al., 2021).

However, when the Dia content exceeds 30 wt%, the polymer matrix may not be sufficient to encapsulate Dia particles. This weakens the intermolecular stress transfer of the polymer, resulting in a reduction in compressive strength and an increase in the crushing rate. In summary, the initial decrease in the crushing rate is attributed to the high interfacial shear strength, crack expansion transfer, and stiffness improvement, while the subsequent increase is due to the weakening of intermolecular stress transfer as the Dia content exceeds a certain threshold (Chaowasakoo and Sombatsompop, 2007, Liang et al., 2017), which is 30 wt% in this case.

The crushing rate of poly(MMA-co-St)/Dia composite beads is much lower compared to that of sand (36 %) and ceramic (10.2 %) proppant (Ma et al., 2019), thereby meeting the requirements of high-pressure working environments in hydraulic fracturing.

3.4. Thermal analysis

The prepared ULW proppant should retain high thermal stability in order to effectively withstand the high-temperature working environment underground (Michael et al., 2020, Danso et al., 2021, Liao et al., 2022). Therefore, the thermal properties of the samples are assessed through thermogravimetry (TGA) and differential scanning calorimetry

(DSC) analysis.

The TGA curves demonstrate that the poly(MMA-co-St), poly(MMA-co-St)/20 wt% Dia, poly(MMA-co-St)/30 wt% Dia, and poly(MMA-co-St)/40 wt% Dia samples exhibit weight losses of no more than 5 % at temperatures of 347, 356, 362, and 372 °C, respectively (Fig. 6a). TGA results also indicate that poly(MMA-co-St) undergoes nearly complete decomposition at 450 °C, while noticeable amounts of residue are observed for the poly(MMA-co-St)/20 wt% Dia, poly(MMA-co-St)/30 wt % Dia, and poly(MMA-co-St)/40 wt% Dia, which correspond to the calcined residue of Dia. The detailed values obtained from TGA curves are presented in Table S2 (Supporting Information).

The DTG curves reveal that the poly(MMA-co-St) has a maximum weight loss temperature of 407.7 °C, while for the poly(MMA-co-St)/Dia with 20, 30, and 40 wt% Dia, this value increases to 410.6, 414.2, and 416.7 °C, respectively (Fig. 6b). The maximum weight loss temperature of the composite increases with the addition of Dia for the following reasons. (1) Thermal barrier effect: The thermally stable Dia serves as a thermal barrier in the composite by hindering the diffusion of volatile decomposition products, thereby increasing the temperature required for weight loss to occur. (2) Improved thermal stability: The incorporation of Dia into the composite enhances its thermal stability. Dia particles are well dispersed within the poly(MMA-co-St) matrix, creating a complex pathway that restricts the movement of volatile decomposition products. As a result, there is less weight loss compared to pure poly (MMA-co-St). (3) Enhanced intermolecular interactions: The presence of Dia promotes intermolecular interactions between the poly(MMA-co-St) matrix and the Dia particles. These interactions strengthen the composite structure, making it more resistant to thermal degradation and increasing the maximum weight loss temperature (Bhanvase et al., 2012, Chen et al., 2021). The similar results can be seen in the composites of PS/Dia (Figure S9, Supporting Information) and PMMA/Dia (Figure S10, Supporting Information). Overall, the Dia enhances the thermal stability of the composite by serving as a thermal barrier, enhancing intermolecular interactions, and hindering the diffusion of volatile decomposition products.

The DSC curves in Fig. 6c display that the glass transition temperature (T_g) of poly(MMA-co-St) is 112.5 °C. With the incorporation amount of Dia increases to 20 and 40 wt%, the T_g of the composite also escalates to 114.8 and 120.5 °C, respectively. The increase in the T_g of the composite after adding diatomite can be attributed to several factors. (1) Filler-polymer interaction: The inorganic filler of Dia can establish robust interactions with the copolymer matrix. These interactions impede the mobility of polymer chains, resulting in an increase in T_g . (2) Reinforcement effect: The rigid and porous structure of diatomite reinforces the copolymer matrix, restricting polymer chain movement and increasing the composite's T_g . (3) Increased crosslinking: The addition of Dia promotes crosslinking reactions within the copolymer matrix, increasing network density and restricting molecular motion, resulting in a higher T_g . (4) Reduced free volume: Dia particles occupy space within the polymer matrix, thereby reducing the available free volume for polymer chain movement. This reduction in free volume results in an

increase in the T_g of the composite (Huang et al., 2012, Alhaleb et al., 2017). The incorporation of Dia as an inorganic filler has also been demonstrated to enhance the T_g of polymer composites, as evidenced by the DSC curves of PS/Dia and PMMA/Dia (Figure S11, Supporting Information). Overall, the addition of Dia improves the thermal stability of the composite material, as indicated by the increased T_g . The enhanced thermal stability of the poly(MMA-co-St)/Dia will facilitate its application as proppants in deep oil reservoirs.

3.5. Acid solubility and turbidity

The obtained poly(MMA-co-St)/Dia composite beads should maintain low acid solubility and turbidity in order to adapt well to the harsh acidic working environment underground (Michael et al., 2020, Danso et al., 2021, Liao et al., 2022). Fig. 7a demonstrates the acid solubility of the synthesized composite beads. The poly(MMA-co-St) exhibits the lowest acid solubility since the polymeric materials possess excellent chemical resistance (Zhang et al., 2015, Liang et al., 2017). After incorporating inorganic Dia, the acid solubility of the composite beads is enhanced due to the reaction between Dia and acid (Zhang et al., 2015, Ren et al., 2019). However, even when the Dia content reaches 40 wt%, the acid solubility of poly(MMA-co-St)/Dia composite beads (4.03 %) remains lower than that of sand (4.59 %) and ceramic (5.89 %) proppant (Chen et al., 2015).

Low turbidity is also a crucial parameter for proppants, as any small debris shed from the proppant may fill the gaps between particles, resulting in reduced flow conductivity. The turbidity of the composite increases as the Dia content rises (Fig. 7b), which is caused by brittle inorganic Dia particles detaching from the beads. The turbidity of poly (MMA-co-St)/Dia increases to 33 NTU when the Dia content reaches 40 wt%, which is still lower than that of sand (100 NTU) and ceramic (80 NTU) proppants (Chen et al., 2015). The low acid solubility and low turbidity of poly(MMA-co-St)/Dia enable it to maintain long-term flow conductivity of reservoirs, thereby enhancing the efficiency of oil and gas extraction.

The apparent density, crushing rate, acid solubility, turbidity, and sphericity of the obtained poly(MMA-co-St)/Dia composite proppant are compared with those of traditional proppant and other ULW proppants (Table 1). The traditional sand and ceramic proppants are unsuitable for hydraulic fracturing due to their high density, high crushing rate, high acid solubility, high turbidity, and low sphericity (Michael et al., 2020, Danso et al., 2021). The nutshell-based proppant exhibits relatively low density, yet it demonstrates high crushing rate, high acid solubility, and high turbidity (Zoveidavianpoor and Gharibi, 2016).

The poly(MMA-co-St)/Dia composite proppant in our work, however, display not only an ultra-low density, but also a low crushing rate, low acid solubility, low turbidity, and high sphericity. Although the acid solubility and turbidity are not reported for many other polymer composite based proppants, the poly(MMA-co-St)/Dia composite proppant still exhibit a relatively low acid solubility and low turbidity. The aforementioned advantages make poly(MMA-co-St)/Dia composite

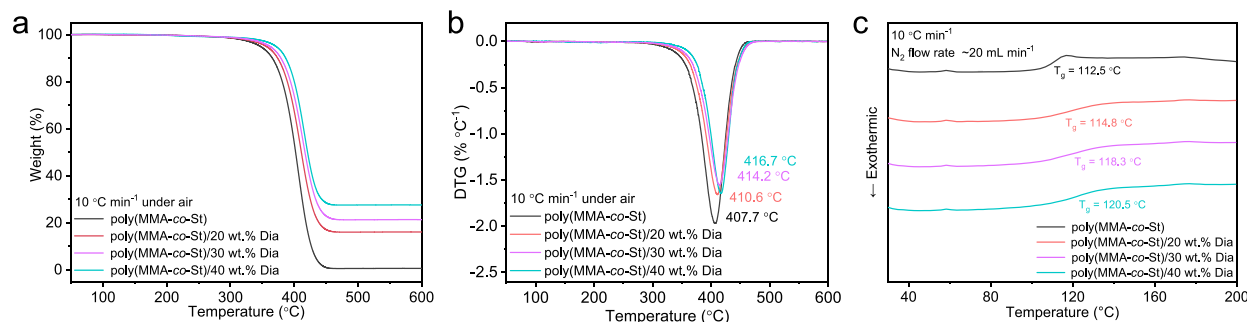


Fig. 6. (a) TGA, (b) DTG, and (c) DSC curves of poly(MMA-co-St), poly(MMA-co-St)/20 wt% Dia, and poly(MMA-co-St)/40 wt% Dia.

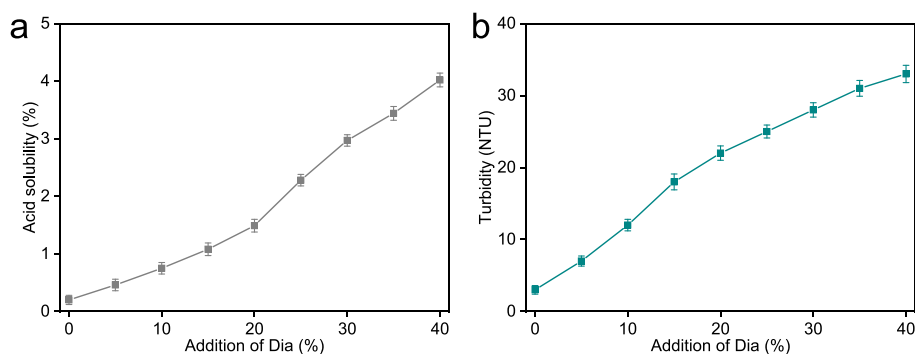


Fig. 7. (a) Acid solubility and (b) turbidity of poly(MMA-co-St)/Dia composite beads containing different amounts of Dia.

Table 1

Comparison of different proppants.

Proppant	Apparent density (g cm^{-3})	Crushing rate (%)	Acid solubility (%)	Turbidity (NTU)	Sphericity	Ref.
Sand	2.65	36	4.59	100	0.65	(Chen et al., 2015)
Ceramic	3.25	10.2	5.89	80	0.85	(Chen et al., 2015)
Nutshell	1.25	7.0	47	188	0.7	(Zoveidavianpoor and Gharibi, 2016)
PMMA/Graphite	1.06	3.0	/	/	> 0.9	(Chen et al., 2015)
PMMA/SF	1.16	2.2	2	/	> 0.9	(Wang et al., 2015)
PMMA/FA	1.05	3.0	/	54	> 0.9	(Zhang et al., 2015)
PS/Graphite	1.05	1.3	/	/	> 0.9	(Han et al., 2014)
PS/CB	1.08	2.0	/	/	> 0.9	(Ma et al., 2019)
PS/SF	1.05	1.0	2.26	/	> 0.9	(Liang et al., 2017)
Poly(MMA-co-St)/Dia	1.025~1.213	0.99	4.03	33	> 0.9	This work

proppants suitable for environmentally friendly slick water fracturing (Liang et al., 2016).

4. Conclusions

The ULW proppant of poly(MMA-co-St)/Dia has been designed and synthesized through clay modification and copolymerization. The composite beads exhibit a low density ranging from 1.025 to 1.213 g cm^{-3} , along with a high sphericity exceeding 0.9. The strong bonding between the poly(MMA-co-St) matrix and rigid Dia restricts the movement of the molecular chain, making the poly(MMA-co-St)/Dia more resistant to crushing. The copolymerization of MMA and St overcomes the limitations of the monomers through their synergistic effect, achieving not only enhanced compressive strength but also improved chemical resistance. The thermal barrier of Dia enhances crosslinking reactions within the copolymer matrix, leading to an increased network density and restricted molecular motion of poly(MMA-co-St)/Dia, resulting in improved thermal stability. In addition, the obtained poly(MMA-co-St)/Dia composite proppant exhibits much lower acid solubility (4.03 %) and turbidity (33 NTU) compared to traditional proppants. Overall, the obtained poly(MMA-co-St)/Dia composite beads hold great potential as a substitute for traditional proppants in hydraulic fracturing for oil and gas exploitation.

CRediT authorship contribution statement

Yuan Zhao: Investigation, Writing – original draft. **Tao Chen:** Conceptualization, Writing – review & editing. **Li Chen:** Data curation, Writing – review & editing. **Guowen Hu:** Supervision, Writing – review & editing. **Xiaobing Han:** Data curation, Writing – review & editing. **Tian Liang:** Formal analysis, Writing – review & editing. **Jie Gao:** Formal analysis, Writing – review & editing.

Declaration of Competing Interest

The authors declare that they have no known competing financial

interests or personal relationships that could have appeared to influence the work reported in this paper.

Acknowledgments

This work was financially supported by the National Natural Science Foundation of China (51903080), Foundation of Hubei Provincial Department of Education (Q20222802, D20212801, B2021223), and Scientific Research Foundation of Hubei University of Science and Technology (2021ZX06, 2021ZX15, 2022T03, 2022ZX10, 2022ZX13, BK202314).

Appendix A. Supplementary material

Supplementary data to this article can be found online at <https://doi.org/10.1016/j.arabjc.2024.105768>.

References

- Alharez, A.O., Md Akil, H., Ahmad, Z.A., 2017. Influences of NBR/Al₂O₃/YSZ as fillers for PMMA composite on the thermal properties. *Mater. Sci. Forum.* 888, 198–202. <https://doi.org/10.4028/www.scientific.net/MSF.888.198>.
- Bernardo, V., Martín-de León, J., Laguna-Gutiérrez, E., et al., 2017. PMMA-sepiolite nanocomposites as new promising materials for the production of nanocellular polymers. *Eur. Polym. J.* 96, 10–26. <https://doi.org/10.1016/j.eurpolymj.2017.09.002>.
- Bhanvase, B.A., Pinjari, D.V., Gogate, P.R., et al., 2012. Synthesis of exfoliated poly(styrene-co-methyl methacrylate)/montmorillonite nanocomposite using ultrasound assisted in situ emulsion copolymerization. *Chem. Eng. J.* 181–182, 770–778. <https://doi.org/10.1016/j.cej.2011.11.084>.
- Chaowasakoo, T., Sombatsompop, N., 2007. Mechanical and morphological properties of fly ash/epoxy composites using conventional thermal and microwave curing methods. *Compos. Sci. Technol.* 67, 2282–2291. <https://doi.org/10.1016/j.compscitech.2007.01.016>.
- Chaudhary, V., Sharma, S., 2019. Suspension polymerization technique: parameters affecting polymer properties and application in oxidation reactions. *J. Polym. Res.* 26, 102. <https://doi.org/10.1007/s10965-019-1767-8>.
- Chen, T., Wang, Y., Yan, C., et al., 2015. Preparation of heat resisting poly(methyl methacrylate)/graphite composite microspheres used as ultra-lightweight proppants. *J. Appl. Polym. Sci.* 132, 41924. <https://doi.org/10.1002/app.41924>.

- Chen, T., Sang, Y., Zhou, Y., et al., 2021. Facile and controllable preparation of poly(St-co-MMA)/FA microspheres used as ultra-lightweight proppants. *Materials*. 14, 7390. <https://doi.org/10.3390/ma14237390>.
- Danso, D.K., Negash, B.M., Ahmed, T.Y., et al., 2021. Recent advances in multifunctional proppant technology and increased well output with micro and nano proppants. *J. Pet. Sci. Eng.* 196, 108026 <https://doi.org/10.1016/j.petrol.2020.108026>.
- Feng, Y.-C., Ma, C.-Y., Deng, J.-G., et al., 2021. A comprehensive review of ultralightweight proppant technology. *Pet. Sci.* 18, 807–826. <https://doi.org/10.1007/s12182-021-00559-w>.
- Fjaestad, D., Tomac, I., 2019. Experimental investigation of sand proppant particles flow and transport regimes through narrow slots. *Powder Technol.* 343, 495–511. <https://doi.org/10.1016/j.powtec.2018.11.004>.
- Fu, L., Zhang, G., Ge, J., et al., 2016. Surface modified proppants used for proppant flowback control in hydraulic fracturing. *Colloids Surf A Physicochem Eng Asp* 507, 18–25. <https://doi.org/10.1016/j.colsurfa.2016.07.039>.
- Gaurav, A., Dao, E.K., Mohanty, K.K., 2010. Ultra-lightweight proppants in shale gas fracturing. *SPE Unconvent. Resour. Conference/Gas Technol. Symposium* 138319. <https://doi.org/10.2118/138319-MS>.
- Gaurav, A., Dao, E.K., Mohanty, K.K., 2012. Evaluation of ultra-light-weight proppants for shale fracturing. *J. Pet. Sci. Eng.* 92–93, 82–88. <https://doi.org/10.1016/j.petrol.2012.06.010>.
- Gutiérrez Moreno, J.J., Pan, K., Wang, Y., et al., 2020. Computational study of APTES Surface functionalization of diatom-like amorphous SiO₂ Surfaces for heavy metal adsorption. *Langmuir* 36, 5680–5689. <https://doi.org/10.1021/acs.langmuir.9b03755>.
- Han, X., Cheng, Q., Bao, F., et al., 2014. Synthesis of low-density heat-resisting polystyrene/graphite composite microspheres used as water Carrying fracturing proppants. *Polym.-Plast. Technol. Eng.* 53, 1647–1653. <https://doi.org/10.1080/03602259.2014.919648>.
- Huang, N., Chen, Z., Liu, H., et al., 2012. Thermal stability and degradation kinetics of poly(methyl methacrylate)/sepiolite nanocomposites by direct melt compounding. *J. Macromol. Sci., Part B* 52, 521–529. <https://doi.org/10.1080/00222348.2012.716318>.
- Huang, W., Li, D., Jiang, B., et al., 2010. Branching copolymerization of styrene and methyl methacrylate with divinylbenzene. *Iran. Polym. J.* 19, 589–598. WOS: 000281830500003.
- Liang, F., Sayed, M., Al-Muntasheri, G.A., et al., 2016. A comprehensive review on proppant technologies. *Petroleum*. 2, 26–39. <https://doi.org/10.1016/j.petlm.2015.11.001>.
- Liang, T., Yan, C., Zhou, S., et al., 2017a. Silica fume reinforced polystyrene-based composite particles used as ultra-light weight proppants in hydraulic fracturing. *Mater. Res. Express* 4, 115306. <https://doi.org/10.1088/2053-1591/aa98a7>.
- Liang, T., Yan, C., Zhou, S., et al., 2017b. Carbon black reinforced polymethyl methacrylate (PMMA)-based composite particles: preparation, characterization, and application. *J. Geophys. Eng.* 14, 1225–1232. <https://doi.org/10.1088/1742-2140/aabe7e>.
- Liao, Z., Li, X., Ge, L., et al., 2022. Lightweight proppants in unconventional oil and natural gas development: a review. *Sustain. Mater. Technol.* 33, e00484.
- Ma, R., Tang, W., Hu, P., et al., 2019b. Fabrication of low-density heat-resistance polystyrene/carbon black composite microspheres used as hydraulic fracturing proppant. *Mater. Express* 9, 150–158. <https://doi.org/10.1166/mex.2019.1478>.
- Ma, H., Tian, Y., Li, G., 2019a. Effects of sintering temperature on microstructure, properties, and crushing behavior of ceramic proppants. *Int. J. Appl. Ceram. Technol.* 16, 1450–1459. <https://doi.org/10.1111/ijac.13204>.
- Mao, S., Zhang, Z., Chun, T., et al., 2020. Field-scale numerical investigation of proppant transport among multicluster hydraulic fractures. *SPE J.* 26, 307–323.
- Michael, F.M., Krishnan, M.R., Li, W., et al., 2020. A review on polymer-nanofiller composites in developing coated sand proppants for hydraulic fracturing. *J. Nat. Gas Sci. Eng.* 83, 103553 <https://doi.org/10.1016/j.jngse.2020.103553>.
- Pangilan, K.D., de Leon, A.C.C., Advincula, R.C., 2016. Polymers for proppants used in hydraulic fracturing. *J. Pet. Sci. Eng.* 145, 154–160. <https://doi.org/10.1016/j.petrol.2016.03.022>.
- Posey, D., Strickland, B., 2005. The effect of using a lightweight proppant in treatment of a low-permeability, dry gas reservoir: a case study. *SPE Eastern Regional Meeting*. 97998 <https://doi.org/10.2118/97998-MS>.
- Ramlan, A.S., Zin, R.M., Abu Bakar, N.F., et al., 2022. Characterisation of graphene oxide-coated sand for potential use as proppant in hydraulic fracturing. *Arab. J. Geosci.* 15, 1126. <https://doi.org/10.1007/s12517-022-10384-z>.
- Ren, Q., Ren, Y., Li, H., et al., 2019. Preparation and characterization of high silicon ceramic proppants using low grade bauxite and fly ash. *Mater. Chem. Phys.* 230, 355–361. <https://doi.org/10.1016/j.matchemphys.2019.04.009>.
- Salisu, A., Sanagi, M.M., Abu Naim, A., et al., 2015. Alginate graft polyacrylonitrile beads for the removal of lead from aqueous solutions. *Polym. Bull.* 73, 519–537. <https://doi.org/10.1007/s00289-015-1504-3>.
- Spurr, N.B., Hudson, H., Hughes, B., 2017. Ultra-light weight proppant and pumping design lead to greater conductive fracture area in unconventional reservoirs. *SPE Oil and Gas India Conference and Exhibition*. 185435 <https://doi.org/10.2118/185435-MS>.
- Sun, M., Pan, C., 2010. Formation of hyperbranched polymers in atom transfer radical copolymerization of MMA and DVB. *Sci. China Chem.* 53, 2440–2451. <https://doi.org/10.1007/s11426-010-4155-0>.
- Tasqué, J.E., Vega, I.N., Marco, S., et al., 2021. Ultra-light weight proppant: synthesis, characterization, and performance of new proppants. *J. Nat. Gas Sci. Eng.* 85, 103717 <https://doi.org/10.1016/j.jngse.2020.103717>.
- Wang, Y., Chen, T., Yan, C., 2015. Reinforced performances of polymethyl methacrylate/silica fume composite spherical particles used as ultra-lightweight proppants. *J. Reinf. Plast. Compos.* 34, 672–683. <https://doi.org/10.1177/0731684415577236>.
- Wu, X., Zhang, J., Zhang, L., et al., 2022. Thermal stability of APTES surface modified nano SiO₂ insulating oil. *J. Mol. Liq.* 366, 120228 <https://doi.org/10.1016/j.molliq.2022.120228>.
- Xu, X., Yang, Y., Guan, Y., et al., 2023. Persistent free radicals on carbon nanotubes and their catalytic effect on benzoyl peroxide decomposition. *Carbon* 201, 473–482. <https://doi.org/10.1016/j.carbon.2022.09.028>.
- Yao, S., Chang, C., Hai, K., et al., 2022. A review of experimental studies on the proppant settling in hydraulic fractures. *J. Pet. Sci. Eng.* 208, 109211 <https://doi.org/10.1016/j.petrol.2021.109211>.
- Zhang, S., So, L.L.C., Faucher, S., et al., 2016. Polymer coating over solid particles with in situ thermal curing. *Ind. Eng. Chem. Res.* 55, 5574–5584. <https://doi.org/10.1021/acs.iecr.6b00376>.
- Zhang, Y., Yan, C., Chen, T., et al., 2015. Ultra-lightweight composite proppants prepared via suspension polymerization. *J. Compos. Mater.* 50, 2823–2831. <https://doi.org/10.1177/0021998315613128>.
- Zheng, R., Ren, Z., Gao, H., et al., 2018. Effects of calcination on silica phase transition in diatomite. *J. Alloy. Compd.* 757, 364–371. <https://doi.org/10.1016/j.jallcom.2018.05.010>.
- Zoveidavidanpoor, M., Gharibi, A., 2016. Characterization of agro-waste resources for potential use as proppant in hydraulic fracturing. *J. Nat. Gas Sci. Eng.* 36, 679–691. <https://doi.org/10.1016/j.jngse.2016.10.045>.